*Wael. H. Alsaedi[1], Ahmed Al-Amiery[2,3,]**

[1]Department of Chemistry, College of Science, Taibah University, Madinah, Saudi Arabia, [2]Science and Technology Parks, Al-Ayen Iraqi University, AUIQ, An Nasiriyah, Thi Qar, Iraq, [3]Energy and Renewable Energies Center, University of Technology, Baghdad, Iraq

Scientific paper
ISSN 0351-9465, E-ISSN 2466-2585
https://doi.org/10.62638/ZasMat1555

Zastita Materijala 67 ()
(2026)

Eco-compatible protection of mild steel in 1 M HCl using N-(ortho-anisyl)piperazine: A synergistic electrochemical and DFT approach

ABSTRACT

The corrosion behavior of mild steel in 1 M HCl was investigated in the presence of N-(ortho-anisyl)piperazine (NAP), a heterocyclic organic inhibitor, using electrochemical methods, surface analysis, and quantum chemical modeling. Potentiodynamic polarization (PDP) studies revealed that NAP acts as a mixed-type inhibitor, achieving up to 84% inhibition efficiency at 0.5 mM concentration. Adsorption of NAP on the steel surface followed Langmuir isotherm behavior, indicating monolayer coverage and spontaneous adsorption, supported by a negative Gibbs free energy of –30.03 kJ·mol⁻¹. Scanning electron microscopy (SEM) confirmed a significant reduction in surface corrosion features in the presence of NAP. Density functional theory (DFT) calculations showed favorable electronic descriptors, including a high HOMO (–7.927 eV), low LUMO (1.307 eV), and a positive electron transfer fraction (ΔN = 0.398), supporting strong donor–acceptor interactions with the mild steel surface. Molecular mechanics parameters indicated stable structural flexibility ideal for adsorption. A comprehensive inhibition mechanism involving both physisorption and chemisorption is proposed. The study highlights NAP as an eco-friendly and efficient corrosion inhibitor, offering a synergistic understanding of inhibition through experimental and theoretical approaches.

Keywords: *Piperazine, potentiodynamic polarization, corrosion inhibitor, SEM, DFT*

1. INTRODUCTION

The corrosion of mild steel in acidic environments is a persistent challenge in the petrochemical, energy, and manufacturing sectors, with serious economic and safety implications. Globally, the annual cost of corrosion surpasses US $2.5 trillion, amounting to nearly 3.4% of the world's GDP, according to NACE International [1,2]. Among the various corrosion mechanisms, acid-induced uniform corrosion, especially in hydrochloric acid (HCl) is particularly severe during processes such as acid pickling, descaling, cleaning, and oil-well acidizing. The demand for highly efficient, eco-compatible corrosion inhibitors that can operate effectively in such aggressive media continues to grow, especially given tightening environmental regulations [3,4]. Organic compounds containing heteroatoms (N, O, S) and conjugated π-systems are widely recognized as effective corrosion inhibitors due to their ability to adsorb on metallic surfaces and form protective films that suppress both anodic and cathodic reactions [5,6]. Among these, piperazine-based molecules have emerged as a promising class, owing to their electron-donating nitrogen atoms, flexible structure, and favorable adsorption geometry. Substituent modifications on the piperazine ring further allow tuning of electronic and steric properties, thereby enhancing inhibition efficiency. One such modification of interest is the incorporation of the ortho-anisyl (2-methoxyphenyl) group. The methoxy substituent, through its +M (mesomeric) effect, enriches the electron density of the aromatic ring and provides an additional coordination site via its oxygen atom [7,8].

NAP, which integrates this functional group with a piperazine backbone, thus represents an electronically rich yet synthetically simple molecule. However, despite its potential, NAP remains largely unexplored in the context of corrosion inhibition. Mild steel, the material of focus in this study, is extensively used across industries due to its low cost, weldability, and strength. In 1 M HCl, it undergoes active dissolution facilitated by chloride ions, with iron oxidation at the anode and hydrogen evolution at the cathode [10,11]. The high corrosion

*Corresponding author: Ahmed Al-Amiery
E-mail: dr.ahmed1975@gmail.com
Paper received: 26.08.2025.
Paper cottected: 28.04.2026.
Paper accepted: 07.05.2026.

rates necessitate the use of inhibitors to mitigate metal loss and maintain structural integrity. Historically, inorganic inhibitors such as chromates and nitrites were widely used but have fallen out of favor due to toxicity concerns. This has prompted the search for "green" inhibitors molecules that are biodegradable, low in toxicity, and sustainable [12–15]. Piperazine derivatives meet many of these criteria, and previous studies have reported their high inhibition efficiencies when suitably functionalized [16–19]. Nevertheless, a systematic investigation of NAP, particularly with a focus on its electronic structure and adsorption mechanism, is still absent from the literature. In this context, potentiodynamic polarization (PDP) provides critical insight into inhibition performance by measuring corrosion current density, corrosion potential, and Tafel slopes. When paired with surface morphology analysis (via SEM), and density functional theory (DFT) simulations, it becomes possible to build a complete mechanistic picture of how the inhibitor interacts with the metal surface at the molecular level [20–25]. Despite the progress in individual techniques, most previous studies have failed to integrate all three pillars electrochemical evaluation, surface characterization, and theoretical modelling into a unified corrosion inhibition assessment. Additionally, the specific influence of the ortho-methoxy substituent on adsorption geometry and surface coverage remains inadequately understood. The primary aim of this study is to evaluate NAP (Figure 1) as an environmentally friendly and effective corrosion inhibitor for mild steel in 1 M HCl. Through a synergistic methodology combining potentiodynamic polarization, surface analytical techniques (SEM), and DFT calculations, we aim to elucidate its inhibition mechanism, quantify adsorption strength, and identify the key structural features responsible for its performance. This integrated approach contributes to the rational design of green corrosion inhibitors based on structure–activity relationships.

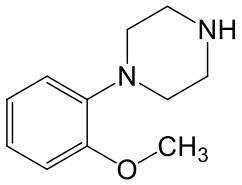

Figure 1. The chemical structure of NAP

2. EXPERIMENTAL SECTION

2.1. Materials and Reagents

The corrosion inhibitor *NAP* was procured in high purity from a commercial supplier (Sigma-Aldrich, Malaysia) and used without any further purification. Analytical-grade reagents were used throughout the study. The purity of NAP was confirmed by thin-layer chromatography (TLC) on silica gel to ensure its suitability for electrochemical and theoretical investigations. Solutions of 1 M hydrochloric acid were prepared by diluting concentrated HCl (Merck, 37%) with deionized water.

2.2. Preparation of Mild Steel Electrodes

Mild steel coupons were used as the working electrode in all corrosion experiments. The nominal composition (in wt.%) was: Fe (99.21), C (0.21), Si (0.38), P (0.09), S (0.05), Mn (0.05), and Al (0.01). Each sample was mechanically abraded using successive grades of silicon carbide paper (600 to 1200 grit), followed by washing with deionised water, degreasing in acetone, and drying under ambient conditions. The exposed surface area was fixed at 4.5 cm². Surface preparation procedures conformed to ASTM G1-03 guidelines to ensure reproducibility and minimize variability in corrosion testing [26].

2.3. Electrochemical Evaluation

Electrochemical experiments were carried out to assess the inhibition performance of NAP on mild steel corrosion in 1.0 M hydrochloric acid. All measurements were performed using a three-electrode glass cell configuration interfaced with a Gamry Reference 600 potentiostat. The mild steel specimen acted as the working electrode, a saturated calomel electrode (SCE) served as the reference, and a platinum wire was employed as the counter electrode. Test solutions were prepared by dissolving analytical-grade HCl to achieve a 1.0 M concentration, and NAP was introduced in various concentrations (ranging from 0.1 mM to 1.0 mM) to evaluate its concentration-dependent inhibition behavior. The working electrode was immersed in the test solution and left at open circuit for 30 minutes to stabilize its corrosion potential (E_{corr}) before electrochemical testing began. Potentiodynamic polarization (PDP) scans were conducted by sweeping the potential in the range of ±200 mV relative to the stabilized open-circuit potential at a scan rate of 0.5 mV·s^{-1}. This procedure allowed for the determination of critical electrochemical parameters including E_{corr}, corrosion current density (i_{corr}), anodic and cathodic Tafel slopes (β_a and β_c), and the type of inhibition mechanism (anodic, cathodic, or mixed-type). The corrosion current density was extracted by Tafel extrapolation [27] and used to calculate the corrosion rate (C_R) according to the following equation (1):

$$C_R(mm/year) = \frac{0.00327 \times i_{corr} \times M}{n \times \rho} \quad (1)$$

where i_{corr} is the corrosion current density (μA/cm²). M represents the atomic mass of iron (55.85 g/mol), n refers to number of electrons exchanged (n = 2 for Fe → Fe^{2+}), ρ represents the density of mild steel (7.87 g/cm³) and 0.00327 refers to conversion factor.

The inhibition efficiency (IE%) was then calculated using (2):

$$IE\% = \left(1 - \frac{i_{corr}^{inh}}{i_{corr}^{blank}}\right) \times 100 \quad (2)$$

Where i_{corr}^{inh} is the corrosion current density in the absence of NAP and i_{corr}^{blank} refers to the corrosion current density in the presence of the inhibitor

All electrochemical measurements were repeated a minimum of three times to ensure reproducibility, and only the average values were considered for data interpretation. This rigorous testing protocol ensured high accuracy in quantifying the corrosion mitigation capability of NAP under acidic conditions.

2.4. Computational Study

To elucidate the molecular-level inhibition behavior, density functional theory (DFT) calculations were performed using the GAMESS software package. The B3LYP/6-31G(d) level has been widely validated for studying organic corrosion inhibitors and provides reliable electronic descriptors for adsorption analysis, particularly for predicting frontier orbital energies and reactivity indices. Key electronic descriptors were extracted, including E_{HOMO} (eV) which represents to the highest occupied molecular orbital energy, whereas the E_{LUMO} (eV) refers to the lowest unoccupied molecular orbital energy, ΔE ($E_{\mathrm{LUMO}} - E_{\mathrm{HOMO}}$) Energy gap and μ (Debye) refers to the dipole moment [28]. Additional indices were calculated (3-7):

Ionization potential (I): $I = -E_{HOMO}$ (3)

Electron affinity (A): $A = -E_{LUMO}$ (4)

Electronegativity (χ): $\chi = \frac{I+A}{2}$ (5)

Chemical hardness (η): $\eta = \frac{I-A}{2}$ (6)

Chemical softness (σ): $\sigma = \eta^{-1}$ (7)

Additionally, the electron transfer fraction (ΔN) between the inhibitor and the mild steel surface was computed as follows (8):

$$\Delta N = \frac{7-\chi_{inh}}{2\eta_{inh}} \quad (8)$$

Where χ_{inh} and η_{inh} refer to the electronegativity and hardness of the inhibitor, respectively. For these calculations, the reference values for iron (Fe) were taken as χ_{Fe} = 7 eV and η_{Fe} = 0 eV.

3. RESULTS AND DISCUSSION

3.1. Polarization measurements

Potentiodynamic polarization analysis was performed to investigate the electrochemical behavior of mild steel in 1 M HCl solution in the absence and presence of *NAP* at various concentrations. The polarization curves obtained are depicted in Figure 2, and the corresponding electrochemical parameters, including corrosion potential (E_{corr}), corrosion current density (i_{corr}), anodic and cathodic Tafel slopes (β_a and $-\beta_c$), and inhibition efficiency (IE%), are summarized in Table 1.

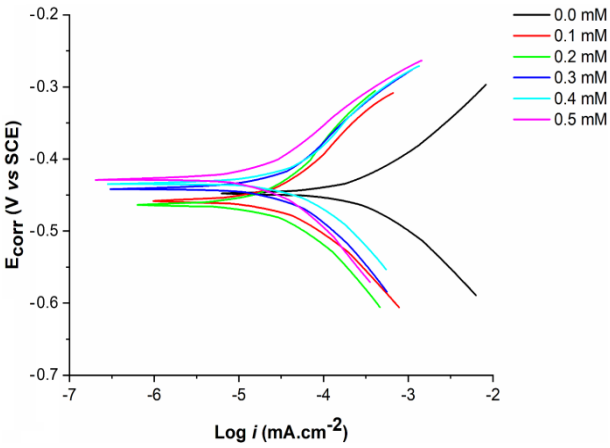

Figure 2. Potentiodynamic polarization curves for mild steel in 1 M HCl in the absence and presence of various concentrations of NAP (0.1–0.5 mM).

Table 1. Electrochemical parameters derived from Tafel polarization measurements for mild steel in 1 M HCl with and without NAP.

Conc. (mM)	E_{corr} (mV)	i_{corr} ($\mu A\ cm^{-2}$)	β_a (mV dec^{-})	$-\beta_c$ (mV dec^{-})	IE (%)
blank	-480	0.75	95	155	0
0.1	-474	0.54	98	147	28
0.2	-466	0.39	102	142	48
0.3	-459	0.30	106	137	60
0.4	-452	0.19	111	134	74.6
0.5	-449	0.12	114	131	84

In the uninhibited (blank) solution, the corrosion potential of mild steel was observed at –480 mV vs. SCE, with a corresponding corrosion current density of 0.75 μA cm⁻². Upon the addition of NAP, E_{corr} values shifted positively, reaching –449 mV at the highest inhibitor concentration (0.5 mM), indicating a tendency towards anodic polarization. However, the magnitude of the shift was less than 85 mV in all cases, suggesting that NAP functions as a mixed-type inhibitor with a slight anodic preference. A substantial reduction in corrosion current density was observed with increasing NAP concentration. For instance, i_{corr} decreased from 0.75 μA cm⁻² (blank) to 0.12 μA cm⁻² at 0.5 mM, indicating a strong suppression of both anodic metal dissolution and cathodic hydrogen evolution. This trend directly correlates with the enhancement in inhibition efficiency, which improved progressively from 28% at 0.1 mM to 84% at 0.5 mM, highlighting the concentration-dependent protective action of the inhibitor. The values of the anodic (β_a) and cathodic (β_c) Tafel slopes provide further insight into the inhibition mechanism. Both slopes exhibited systematic changes with increasing inhibitor concentration. The anodic slope increased from 95 mV dec⁻¹ in the blank solution to 114 mV dec⁻¹ at 0.5 mM, while the cathodic slope decreased from –155 mV dec⁻¹ to –131 mV dec⁻¹ over the same concentration range. These changes suggest that NAP affects the kinetics of both anodic and cathodic reactions, potentially through adsorption on active sites. The shift in slope values indicates that the inhibitor modifies the surface reaction mechanisms, possibly by altering the activation energy barriers or creating a more compact protective film over time [29,30].

The mixed-type inhibition behavior of NAP is consistent with its molecular structure, which includes electron-rich nitrogen atoms in the piperazine ring and a methoxy-substituted aromatic ring capable of π–d interactions. These functional groups facilitate adsorption onto the mild steel surface via both electrostatic interactions and chemisorption, thereby blocking corrosion-active sites and suppressing electron transfer. The inhibition efficiency (IE%) was calculated from corrosion current densities using the equation (2). The maximum efficiency (84%) achieved at 0.5 mM suggests that NAP forms a dense, stable adsorbed layer on the steel surface, effectively reducing both anodic metal dissolution and cathodic hydrogen evolution. The polarization data confirm that NAP exhibits excellent corrosion inhibition properties in acidic environments. The observed positive shift in E_{corr}, reduction in i_{corr}, and modification of Tafel slopes are consistent with an adsorption-mediated protection mechanism. The progressive increase in IE% with concentration also implies monolayer or near-monolayer formation of inhibitor molecules at the metal–solution interface.

3.2. Langmuir adsorption isotherms

The interaction between NAP molecules and the mild steel surface in 1 M HCl was further investigated using adsorption isotherms. These models help describe the nature and strength of the inhibitor's adsorption onto the metal interface, providing insight into the inhibition mechanism and surface coverage behavior. Among the various models tested, the Langmuir isotherm provided the best correlation with the experimental data, indicating that the adsorption of NAP on the mild steel surface adheres closely to Langmuirian assumptions. The Langmuir isotherm assumes monolayer adsorption, homogeneous surface sites, and also no lateral interaction between adsorbed species [31]. The linearized form of the Langmuir equation is given as in Equation (9):

$$\frac{C_{inh}}{\theta} = \frac{1}{K_{ads}} + C_{inh} \qquad (9)$$

where C_{inh} refers to the concentration of the inhibitor (mol·L⁻¹), θ is the surface coverage (calculated from IE% using θ=IE/100, and K_{ads} represents the equilibrium adsorption constant.

A plot of C_{inh}/θ versus C_{inh} yielded a straight line with a correlation coefficient (R^2) very close to 1 (typically $R^2 > 0.98$), confirming the suitability of the Langmuir model. The slope of the line was nearly unity, and the value of K_{ads} was derived from the intercept. The slope value was equal to 0.596, whereas the intercept was equal to 3.02 × 10⁻⁴ mol·L⁻¹. From the equilibrium constant, the standard Gibbs free energy of adsorption ΔG^o_{ads} was calculated using Equation (10):

$$\Delta G^o_{ads} = -RT\ ln(55.5 \times K_{ads}) \qquad (10)$$

where R equal to 8.314 J·mol⁻¹·K⁻¹ (universal gas constant), T equal to 298 K (absolute temperature), whereas the value 55.5 refers to the molar concentration of water in the solution (mol·L⁻¹).

Langmuir adsorption isotherm plot (Figure 3) for the adsorption of NAP on mild steel in 1 M HCl at 298 K.

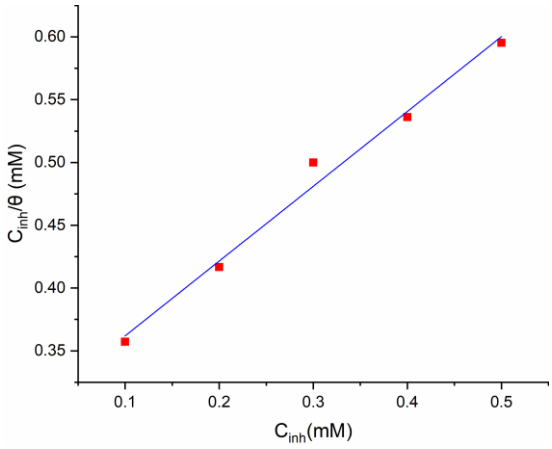

Figure 3. Langmuir Adsorption Isotherm

The linear fit confirms monolayer formation on a homogenous surface, with R^2 = 0.9875 and calculated adsorption free energy (ΔG^o_{ads}) of –30.03 kJ·mol^{-1}, indicating spontaneous and strong adsorption behavior. The calculated was equal to adsorption equilibrium constant (K_{ads}) was equal to 3308 L·mol^{-1}. Furthermore, the negative value of ΔG^o_{ads} indicates a spontaneous adsorption process, and the magnitude (between –20 and –40 kJ/mol) suggests strong physisorption with partial chemisorption [32].

Based on the excellent linear correlation, the slope close to unity, and the realistic values of K_{ads} and ΔG^o_{ads}, the Langmuir adsorption isotherm was confirmed as the most appropriate model for describing the adsorption of NAP on the mild steel surface. This result supports the formation of a stable, compact monolayer of inhibitor molecules that effectively isolates the metal from the corrosive acidic environment.

To ensure the robustness of the adsorption behavior, other isotherms were also evaluated, including Temkin [33] isotherm Equation (11):

$$\theta = \frac{1}{f} ln(K_{ads} C_{ads}) \quad (11)$$

This model accounts for lateral interactions between adsorbed species. However, plots of θ versus ln C yield correlation coefficients which significantly lower (R^2 < 0.98) as in Figure 4, indicating poor fitting. Although the Temkin model shows a strong linear relationship, it is slightly weaker than the Langmuir model. This reinforces that Langmuir isotherm remains the best fit for describing the adsorption behavior of NAP on mild steel in 1 M HCl.

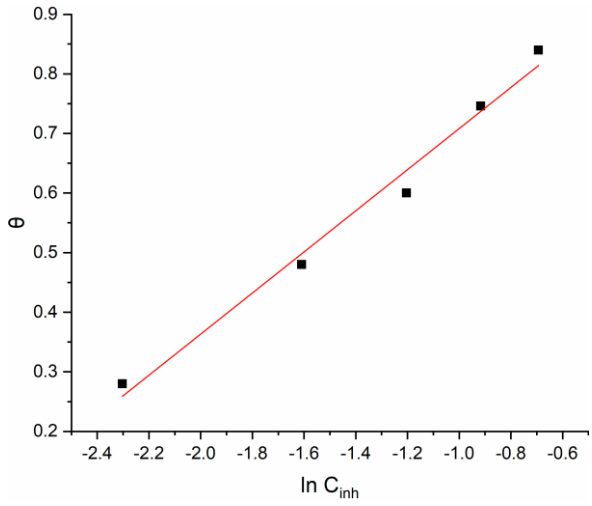

Figure 4. Temkin Adsorption Isotherm

Freundlich Isotherm [34] has empirical model as in Equation (12) assumes a heterogeneous surface.

$$ln\theta = logK_f + \frac{1}{n} logC_{inh} \quad (12)$$

While linearity (Figure 5) was observed to a degree, the R^2 values and statistical parameters were inferior compared to the Langmuir fit. Additionally, the calculated values of the adsorption intensity (1/n) deviated from the expected range for strong interactions (0 < 1/n < 1).

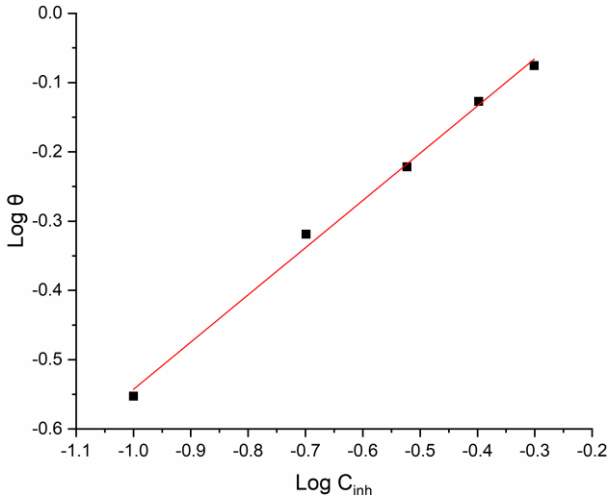

Figure 5. Freundlich Adsorption Isotherm

Despite being an empirical model typically used for heterogeneous surfaces, the Freundlich isotherm shows an even higher correlation than the Temkin models in this case. However, it does not account for monolayer formation, which is consistent with the physical nature of chemisorption observed in the Langmuir interpretation.

The Frumkin model [35] as in Figure 6 includes an interaction parameter **a** to reflect repulsive or attractive interactions between adsorbed molecules.

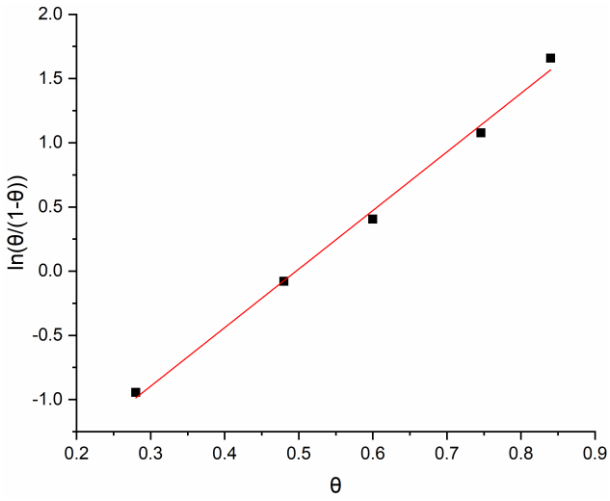

Figure 6. Frumkin Adsorption Isotherm

The deviation from linearity and the inconsistency in computed values of **a** further excluded this model from being the best descriptor of the system as in Equation (13).

$$ln\left(\frac{\theta}{1-\theta}\right) = lnK_{ads} + 2a\theta \quad (13)$$

The Frumkin model accounts for intermolecular interactions (through the parameter *a*), and shows a fit, similar to the Freundlich model. However, the positive slope suggests repulsive interactions between adsorbed NAP molecules, which aligns with partial crowding on the metal surface at higher coverage.

3.3. Surface Morphological Analysis (SEM)

To investigate the morphological changes on the surface of mild steel after exposure to corrosive environments, scanning electron microscopy (SEM) was employed. This technique provides qualitative evidence for corrosion attack and the protective nature of the adsorbed inhibitor film. The SEM micrograph of mild steel immersed in 1 M HCl without inhibitor (Figure 7-a) reveals severe surface degradation. The microstructure exhibits widespread pitting, crevices, and irregular roughness, characteristic of uniform acid corrosion. The high chloride ion concentration in the medium disrupts the passive oxide layer on steel, leading to uncontrolled metal dissolution. These morphological features confirm aggressive corrosion activity in the absence of protective agents [36]. In contrast, the SEM image of mild steel exposed to 1 M HCl containing 0.5 mM of NAP (Figure 7-b) shows a significantly smoother and more uniform surface. The presence of a relatively intact layer with fewer corrosion defects indicates effective inhibition. The absence of pits and the reduction of surface irregularities are attributed to the adsorption of NAP molecules, which form a compact barrier that limits the interaction between chloride ions and the steel substrate.

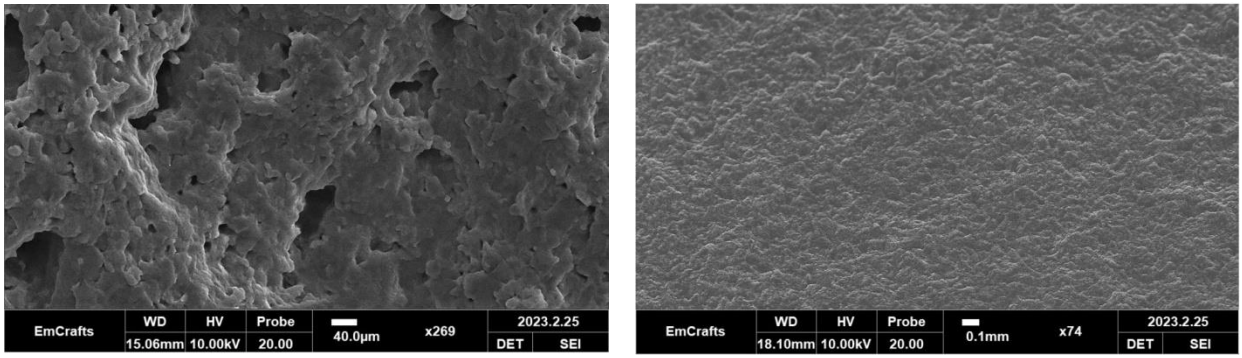

(a) *(b)*

Figure 7. Scanning Electron Microscopy images of mild steel surfaces after 5 hours immersion at 298 K, (a) blank, (b) containing 0.5 mM NAP

These observations agree with the electrochemical data, which demonstrated a substantial decrease in corrosion current density and a high inhibition efficiency at this concentration. The protective film inferred from SEM likely arises from both physical adsorption (physisorption) via electrostatic interactions and chemical adsorption (chemisorption) through electron donation from nitrogen and oxygen atoms in NAP to the steel surface. The improved surface condition in the presence of NAP supports the hypothesis of monolayer formation, as predicted by the Langmuir adsorption isotherm analysis. The ortho-methoxy functional group and the piperazine ring likely contribute to surface coordination, enhancing adhesion to the steel and maintaining surface integrity even under aggressive acidic conditions. The SEM analysis provides compelling visual confirmation of the corrosion-inhibiting effect of NAP. The smoother surface of the inhibited sample demonstrates the successful formation of a protective adsorbed film, validating the inhibitor's performance observed through polarization and adsorption studies.

3.4. Quantum Chemical Analysis of NAP

Quantum chemical calculations provide critical insights into the electronic properties and adsorption behavior of corrosion inhibitors. For this study, density functional theory (DFT) was used to investigate the frontier molecular orbitals specifically the HOMO and LUMO and to evaluate reactivity indices related to the inhibitor's performance on mild steel in acidic media. Figure 8-(a), (b), and (c) represent the optimized geometry, HOMO, and LUMO orbital distributions of NAP, respectively. The molecular conformation as in Figure 8-a is planar, maximizing surface contact and promoting π–π stacking and van der Waals interactions. The electron density of the HOMO is primarily localized on the aromatic anisyl

ring and nitrogen atoms, while the LUMO is distributed over the aromatic and piperazine moieties. This localization suggests that both π-electrons and lone pairs from nitrogen and oxygen atoms are responsible for interaction with the metal surface [37]. The high electron density (Figure 8-b) on the methoxy-phenyl group and nitrogen atoms indicates that these are the active donor sites. Higher HOMO energy corresponds to a stronger ability to donate electrons to the metal's empty d-orbitals, thus favoring chemisorption. The LUMO (Figure 8-c) suggests the molecule's ability to accept back-donated electrons from filled metal orbitals, an essential feature for π-back bonding.

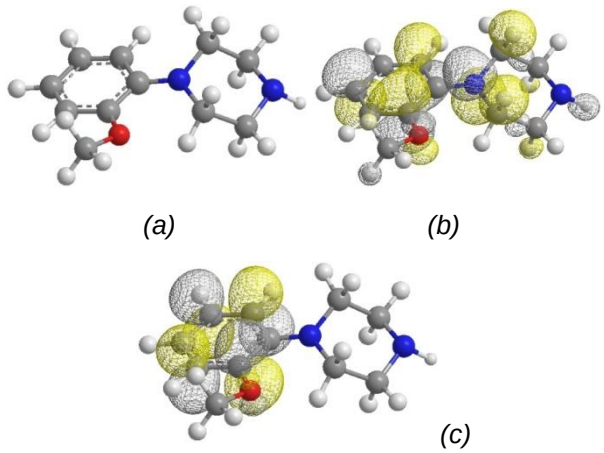

Figure 8. DFT-Optimized Geometry and Frontier Molecular Orbitals of NAP (a) Optimized molecular geometry, (b) HOMO orbital distribution, and (c) LUMO orbital

The calculated quantum chemical parameters (Table 2) provide insight into the reactivity and adsorption behavior of NAP. The relatively high HOMO energy indicates a strong ability of the molecule to donate electrons to the vacant d-orbitals of iron, facilitating chemisorption. Conversely, the LUMO energy reflects the capacity to accept electrons through back-donation mechanisms. The moderate energy gap (ΔE) suggests a balance between molecular stability and reactivity, which is favorable for corrosion inhibition. Furthermore, the positive value of the electron transfer fraction (ΔN) confirms that electron donation from the inhibitor to the metal surface is thermodynamically favorable, supporting strong adsorption. A higher value indicates of ionization potential (I = 7.927 eV) difficulty in losing electrons, which implies good resistance against oxidative degradation. However, the moderate range still allows interaction with metal surfaces. The negative value of electron affinity (A = –1.307 eV) signifies that the LUMO is readily available for back-donation, supporting a synergistic mechanism involving electron donation and acceptance, whereas moderate electronegativity (χ = 3.31 eV) implies a good balance between electron-donating and accepting capabilities, facilitating adsorption onto mild steel. High hardness (η = 4.617 eV) indicates that the molecule is chemically stable and less reactive; however, sufficient softness remains to allow for interaction with the metal, also the softness (σ = 0.217 eV^{-1}) shows the ability of the inhibitor to deform electronically, improving the overlap with metal orbitals [38,39]. Finaly, the positive fraction of electron transfer (ΔN = 0.398) suggests electron transfer from inhibitor to the metal, confirming chemisorption. A value around 0.4 indicates a strong interaction and stable adsorption on the steel surface. The positive ΔN, combined with high HOMO and low LUMO localization near active groups, confirms a strong affinity for the Fe surface, contributing to a stable, protective adsorbed film.

Table 2. Quantum Chemical Parameters of NAP

Parameter	Value
EHOMO (eV)	–7.927
ELUMO (eV)	1.307
Ionization Potential, I (eV)	7.927
Electron Affinity, A (eV)	–1.307
Electronegativity, χ (eV)	3.31
Chemical Hardness, η (eV)	4.617
Chemical Softness, σ (eV^{-1})	0.2166
Electron Transfer Fraction, ΔN	0.3996

The π-system-containing aromatic ring, and balanced steric profile facilitate, strong physisorption via van der Waals and dipolar interactions, also stable chemisorption through lone pair and π-electron donation to vacant Fe d-orbitals and conformational alignment with the metallic surface, maximizing surface coverage and protective film integrity. Although MEP mapping, NBO charge analysis, and Fukui functions can provide deeper insight into reactive sites and electron density distribution, these analyses were not included in the present study and will be considered in future work.

3.5.Proposed Mechanism of Corrosion Inhibition by NAP

The corrosion inhibition behavior of NAP on mild steel in 1 M HCl can be attributed to a synergistic interplay of physicochemical interactions governed by molecular structure, adsorption thermodynamics, electrochemical response, and quantum electronic properties. The inhibition process primarily occurs through the adsorption of NAP molecules onto the mild steel surface, forming a protective barrier that isolates the metal from aggressive chloride and hydrogen ions. This adsorption follows the Langmuir isotherm model, indicating monolayer formation on

homogeneous surface sites. The adsorption mechanism involves both physisorption, through electrostatic interactions between protonated NAP species and the charged metal surface, and chemisorption, through electron donation from the inhibitor to the vacant d-orbitals of iron [40,41]. The molecular structure of NAP plays a key role in its adsorption behavior. The piperazine nitrogen atoms and the oxygen atom of the methoxy group act as electron-rich centers capable of coordinating with iron atoms, while the aromatic π-system facilitates π–d interactions with the metal surface. The presence of the ortho-methoxy substituent enhances electron density across the molecule through its mesomeric (+M) effect, thereby improving the electron-donating ability and strengthening adsorption. Surface analysis using SEM confirms the formation of a smooth and protective film in the presence of NAP, indicating effective surface coverage. As the inhibitor concentration increases, the surface coverage becomes more uniform and compact, reducing the accessibility of corrosive species to the metal interface. This results in the suppression of both anodic metal dissolution and cathodic hydrogen evolution, consistent with the mixed-type inhibition behavior observed in polarization studies. Thermodynamic and quantum chemical analyses further support the proposed mechanism. The negative value of the Gibbs free energy of adsorption confirms the spontaneous nature of the adsorption process, while quantum descriptors such as the HOMO–LUMO energy gap and positive electron transfer fraction (ΔN) indicate favorable electron donation and strong interaction with the metal surface. These combined effects lead to the formation of a stable and adherent protective film that effectively inhibits corrosion.

Figure 9 illustrates the proposed inhibition mechanism of NAP at the metal–solution interface in acidic media. The mild steel surface is initially exposed to aggressive chloride (Cl^-) and hydrogen ions (H^+), which promote anodic dissolution of Fe and cathodic hydrogen evolution. NAP molecules adsorb onto the metal surface through both physisorption and chemisorption. Protonated nitrogen atoms interact electrostatically with negatively charged steel sites, while lone pairs from nitrogen and oxygen atoms coordinate directly with Fe atoms. The adsorbed NAP layer acts as a physical and chemical barrier that blocks H^+ ions and Cl^- from reaching the metal surface, suppressing both anodic ($Fe \rightarrow Fe^{2+} + 2e^-$) and cathodic ($2H^+ + 2e^- \rightarrow H_2$) reactions. The π-electron system of the anisyl ring and lone pairs from heteroatoms enable charge transfer to the vacant d-orbitals of iron, stabilizing the inhibitor–metal complex and reinforcing the protective film [42-44]. Due to the ortho-methoxy substitution and flexible piperazine ring, NAP aligns nearly parallel to the steel surface, maximizing coverage and enhancing surface packing density.

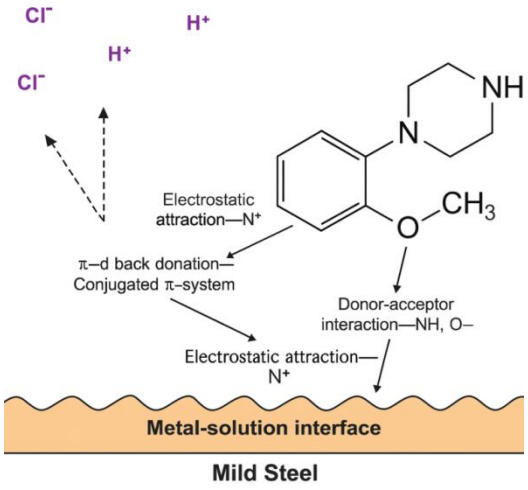

Figure 9. Proposed Mechanism of Corrosion Inhibition by NAP on Mild Steel in 1 M HCl

3.6. Comparison Study

To contextualize the performance of NAP as a corrosion inhibitor for mild steel in acidic environments, a comparative analysis with structurally related compounds and other reported inhibitors is essential. This comparison focuses on inhibition efficiency, adsorption behavior, concentration dependence, and molecular features that influence corrosion protection.

Table 3. Comparison of NAP with other piperazine-based corrosion inhibitors for mild steel in HCl media

Inhibitor	Conc. (mM)	IE (%)	Adsorption Isotherm	ΔG°ads (kJ/mol)	Ref.
NAP	0.5	84	Langmuir	-30.03	Present study
Unsubstituted piperazine	1.0	62	Langmuir	-28.5	[45]
N-phenylpiperazine	1.0	87	Langmuir	-31.2	[46]
N-(para-methoxyphenyl)piperazine	0.5	76	Langmuir	-29.4	[47]
N-(para-chlorophenyl)piperazine	0.5	71	Temkin	-27.8	[48]
1-(4-methoxybenzyl)piperazine	1.0	81	Langmuir	-30.5	[49]

Table 3 presents a comparison of NAP with selected piperazine-based corrosion inhibitors reported in the literature for mild steel in HCl solutions. Notably, NAP demonstrates competitive performance, achieving 84% inhibition efficiency at a relatively low concentration of 0.5 mM. This efficiency surpasses that of unsubstituted piperazine (62% at 1.0 mM) and is comparable to more complex derivatives such as N-phenylpiperazine (87% at 1.0 mM). The ortho-methoxy substituent in NAP appears to enhance its inhibitory properties compared to para-substituted analogs, which typically require higher concentrations to achieve similar protection levels.

The adsorption behavior of NAP follows the Langmuir isotherm, indicating monolayer formation on the steel surface. This behavior is consistent with most piperazine derivatives, as shown in Table 3. The calculated Gibbs free energy of adsorption (-30.03 kJ/mol) suggests a mixed adsorption mechanism involving both physisorption and chemisorption, which is comparable to other effective piperazine-based inhibitors. When compared to non-piperazine heterocyclic compounds containing nitrogen and oxygen atoms (Table 4), NAP demonstrates superior or comparable efficiency at lower concentrations. For instance, benzimidazole derivatives typically require concentrations of 1.0-2.0 mM to achieve inhibition efficiencies of 80-85%, while NAP reaches 84% at only 0.5 mM. This enhanced performance can be attributed to the combined electron-donating effects of the piperazine nitrogen atoms and the ortho-methoxy group, which create multiple active sites for surface adsorption.

Table 4. Comparison of NAP with other heterocyclic corrosion inhibitors for mild steel in 1 M HCl

Inhibitor Type	Example	Conc. mM)	IE (%)	Key Features	Ref.
Piperazine derivative	NAP	0.5	84	Two N atoms, methoxy group	Present study
Imidazole derivative	2-phenylbenzimidazole	1.0	82	N-heterocycle, conjugated system	[50]
Triazole derivative	1,2,4-triazole	5.0	79	Three N atoms, small molecule	[51]
Pyridine derivative	2-aminopyridine	1.0	75	N-heterocycle, amino group	[52]
Quinoline derivative	8-hydroxyquinoline	0.8	88	N,O-heterocycle, chelating ability	[53]

The quantum chemical parameters of NAP further support its effectiveness as a corrosion inhibitor. The HOMO energy (-7.927 eV) is higher than that of many reported inhibitors (typically ranging from -8.5 to -9.5 eV), indicating a greater tendency to donate electrons to the metal surface. The energy gap between HOMO and LUMO (9.234 eV) falls within the optimal range for corrosion inhibitors, balancing reactivity and stability. The electron transfer fraction ($\Delta N = 0.398$) suggests a strong interaction between NAP and the mild steel surface, comparable to other highly efficient inhibitors. The ortho-methoxy substituent in NAP plays a crucial role in its performance. When compared to para-substituted analogs, the ortho position offers steric advantages that promote better surface coverage and more efficient blocking of active corrosion sites. Additionally, the methoxy group's +M effect enhances electron density across the molecule, facilitating stronger interactions with the metal surface. In terms of environmental compatibility, NAP offers advantages over traditional inorganic inhibitors like chromates and nitrites, which are highly toxic. While some organic inhibitors may achieve slightly higher efficiencies, they often contain heavy metals or environmentally persistent functional groups. NAP, with its relatively simple structure and absence of persistent toxic elements, represents a more environmentally sustainable alternative without significantly compromising performance. The concentration dependence of NAP's inhibition efficiency follows a trend similar to other effective organic inhibitors, with efficiency increasing as concentration approaches the critical micelle concentration (CMC). However, NAP achieves its maximum efficiency at a lower concentration compared to many surfactant-type inhibitors, suggesting higher surface activity and more efficient adsorption. In summary, NAP demonstrates competitive performance as a corrosion inhibitor for mild steel in acidic environments, achieving high inhibition efficiency at relatively low concentrations. Its effectiveness can be attributed to the synergistic effects of the piperazine ring and ortho-methoxy substituent, which provide multiple active sites for adsorption and favorable electronic properties. When compared to other inhibitors in its class, NAP offers a balanced combination of efficiency, environmental compatibility, and structural

simplicity, making it a promising candidate for industrial applications.

4. CONCLUSION

The current investigation establishes NAP as a potent and eco-compatible corrosion inhibitor for mild steel in 1 M HCl. Electrochemical polarization studies demonstrated a significant reduction in corrosion current density with increasing NAP concentration, reaching a maximum inhibition efficiency of 84% at 0.5 mM. The inhibitor functions via a mixed-type mechanism, affecting both anodic and cathodic processes. Although electrochemical impedance spectroscopy (EIS) was not included in this study, future investigations will incorporate EIS analysis to provide deeper insight into the interfacial behavior and validate the proposed inhibition mechanism. Adsorption studies confirmed Langmuir isotherm behavior, indicating monolayer formation and strong interaction with the metal surface. SEM imaging provided visual validation of reduced corrosion damage, consistent with the formation of a protective inhibitor film. Quantum chemical and molecular mechanics analyses further elucidated the inhibition mechanism, showing that the methoxy-substituted aromatic ring and nitrogen-containing piperazine core are the active adsorption sites. DFT-derived parameters, including high electronegativity, optimal HOMO–LUMO energy gap, and favorable electron donation characteristics, confirmed the strong adsorption affinity. The proposed inhibition mechanism incorporates both physisorption and chemisorption, enabled by the flexible and electron-rich structure of NAP. Compared to structurally similar piperazine derivatives, NAP offers a balance of high inhibition efficiency, structural simplicity, and environmental safety. The integrated approach combining electrochemistry, surface science, and computational chemistry provides a holistic understanding of NAP's corrosion inhibition performance, supporting its potential application in industrial corrosion protection systems.

5. REFERENCES

[1] G.Jacobson (2016) NACE International's IMPACT Breaks New Ground in the Study of Corrosion Management. Materials Performance, 1;55(4), 28-32

[2] A. Al-Amiery, W.N.R.W. Isahak, W.K. Al-Azzawi (2024) Sustainable corrosion Inhibitors: A key step towards environmentally responsible corrosion control, Ain Shams Engineering Journal, 15(5), 102672. doi: 10.1016/j.asej.2024.102672.

[3] S. Zamindar, S. Mandal, M.Murmu, P. Banerjee (2024) Unveiling the future of steel corrosion inhibition: a revolutionary sustainable odyssey with a special emphasis on N+-containing ionic liquids through cutting-edge innovations. Materials Advances. 5(11), 4563-600. doi: 10.1039/D4MA00156G.

[4] M. Finšgar, J. Jackson (2014) Application of corrosion inhibitors for steels in acidic media for the oil and gas industry: A review, Corrosion Science, 86, 17–41. doi: 10.1016/j.corsci.2014.04.044.

[5] A. Omari Alaoui, M. Messali, W. Elfalleh, B. Hammouti, A. Titi, F. El-Hajjaji (2025) Structure–Activity Relationship of Ionic Liquids for Acid Corrosion Inhibition, International Journal of Molecular Sciences, 26(12), 5750. doi: 10.3390/ijms26125750.

[6] M.A. Dawood, Z.M. Alasady, M.S. Abdulazeez, D.S. Ahmed, G.M. Sulaiman, A.A. Kadhum, L.M. Shaker, A.A. Alamiery (2021) The corrosion inhibition effect of a pyridine derivative for low carbon steel in 1 M HCl medium: Complemented with antibacterial studies, International Journal of Corrosion and Scale Inhibition, 10(4), 1766–1782. doi: 10.17675/2305-6894-2021-10-4-25.

[7] B.S. Mahdi, H.M. Habeeb, I.A. Aziz, M.M. Hanoon, F.F. Sayyid, A.M. Mustafa, T.S. Gaaz, A.H. Jaaz, A.A. Khadom, E. Yousif, A. Alamiery (2024) Understanding the impact of inhibitor concentration, immersion periods, and temperature on the corrosion inhibition of 2-piperazin-1-yl-1,3-benzothiazole in HCl solution, International Journal of Corrosion and Scale Inhibition, 13(2), 1164–1185. doi: 10.17675/2305-6894-2024-13-2-28.

[8] R.D. Salim, N. Betti, M.M. Hanoon, A.A. Al-Amiery (2022) 2-(2,4-Dimethoxybenzylidene)-N-phenyl hydrazinecarbothioamide as an efficient corrosion inhibitor for mild steel in acidic environment, Progress in Color, Colorants and Coatings, 15(1), 45–52. doi. 10.30509/pccc.2021.166775.1105

[9] P.B. Raja, M.G. Sethuraman (2008) Natural products as corrosion inhibitor for metals in corrosive media—a review, Materials Letters, 62(1), 113–116. doi: 10.1016/j.matlet.2007.04.079.

[10] S.A. Abd El-Maksoud, A.S. Fouda (2005) Some pyridine derivatives as corrosion inhibitors for carbon steel in acidic medium, Materials Chemistry and Physics, 93(1), 84–90. doi: 10.1016/j.matchemphys.2005.02.020.

[11] G. Kandasamy (2019) Advances In Corrosion Inhibition Materials And Technologies: A Review, Advanced Materials Letters, 10(4), 231–247. doi: 10.5185/amlett.2019.2199

[12] B.A. Rani, B.B. Basu (2012) Green inhibitors for corrosion protection of metals and alloys: an overview, International Journal of Corrosion, 2012(1), 380217. doi: 10.1155/2012/380217.

[13] G. Gece (2011) Drugs: A review of promising novel corrosion inhibitors, Corrosion Science, 53(12), 3873–3898. doi: 10.1016/j.corsci.2011.08.006.

[14] A. Kadhim, N. Betti, H.A. Al-Bahrani, M.K. Al-Ghezi, T. Gaaz, A.H. Kadhum, A. Alamiery (2021) A mini review on corrosion, inhibitors and mechanism types of mild steel inhibition in an acidic

environment, International Journal of Corrosion and Scale Inhibition, 10(3), 861–884. doi: 10.17675/2305-6894-2021-10-3-3.

[15] N.A. Reza, N.H. Akhmal, N.A. Fadil, M.F. Taib (2021) A review on plants and biomass wastes as organic green corrosion inhibitors for mild steel in acidic environment, Metals, 11(7), 1062. doi: 10.3390/met11071062.

[16] I.B. Obot, N.O. Obi-Egbedi, S.A. Umoren, E.E. Ebenso (2010) Synergistic and antagonistic effects of anions and Ipomoea invulcrata as green corrosion inhibitor for aluminium dissolution in acidic medium, International Journal of Electrochemical Science, 5(7), 994–1007.

[17] M.H. Ahmed, A.A. Al-Amiery, Y.K. Al-Majedy, A.A. Kadhum, A.B. Mohamad, T.S. Gaaz (2018) Synthesis and characterization of a novel organic corrosion inhibitor for mild steel in 1 M hydrochloric acid, Results in Physics, 8, 728–733. doi: 10.1016/j.rinp.2017.12.039.

[18] R. Solmaz (2014) Investigation of adsorption and corrosion inhibition of mild steel in hydrochloric acid solution by 5-(4-Dimethylaminobenzylidene) rhodanine, Corrosion Science, 79, 169–176.

[19] M.A. Quraishi, D. Jamal (2001) Corrosion inhibition of N-80 steel and mild steel in 15% boiling hydrochloric acid by a triazole compound—SAHMT, Materials Chemistry and Physics, 68(1–3), 283–287.

[20] E. McCafferty (2005) Validation of corrosion rates measured by the Tafel extrapolation method, Corrosion Science, 47(12), 3202–3215. doi: 10.1016/j.corsci.2005.05.046.

[21] A. Popova, E. Sokolova, S. Raicheva, M. Christov (2003) AC and DC study of the temperature effect on mild steel corrosion in acid media in the presence of benzimidazole derivatives, Corrosion Science, 45(1), 33–58. doi: 10.1016/S0010-938X(02)00072-0.

[22] K.F. Khaled (2010) Studies of iron corrosion inhibition using chemical, electrochemical and computer simulation techniques, Electrochimica Acta, 55(22), 6523–6532. doi: 10.1016/j.electacta.2010.06.027.

[23] K.F. Al-Azawi, S.B. Al-Baghdadi, A.Z. Mohamed, A.A. Al-Amiery, T.K. Abed, S.A. Mohammed, A.A. Kadhum, A.B. Mohamad (2016) Synthesis, inhibition effects and quantum chemical studies of a novel coumarin derivative on the corrosion of mild steel in a hydrochloric acid solution, Chemistry Central Journal, 10(1), 23.

[24] E.E. Ebenso, C. Verma, L.O. Olasunkanmi, E.D. Akpan, D.K. Verma, H. Lgaz, L. Guo, S. Kaya, M.A. Quraishi (2021) Molecular modelling of compounds used for corrosion inhibition studies: a review, Physical Chemistry Chemical Physics, 23(36), 19987–20027. doi: **10.1039/D1CP00244A**.

[25] H.K. Thabet, J.M. AlGhamdi, H.A. Mohammed, M.A. Elsaid, A.M. Ashmawy (2023) Anticorrosion agents for carbon steel in acidic environments: Synthesis and quantum chemical analysis of new Schiff base compounds with benzylidene, ACS Omega, 8(42), 39770–39782. doi: 10.1021/acsomega.3c05790.

[26] E.C. Freire, A.T. García, C. Redroban, J.C. Vega, F.G. Rodriguez (2024) Efficiency of conventional method of protection against corrosion in ASTM A36 steels in saline medium, ESPOCH Congresses: The Ecuadorian Journal of STEAM, 3(3), 179–192. doi: 10.18502/espoch.v3i3.16621

[27] N.D. Nam, P. Van Hien, N.T. Hoai, V.T. Thu (2018) A study on the mixed corrosion inhibitor with a dominant cathodic inhibitor for mild steel in aqueous chloride solution, Journal of the Taiwan Institute of Chemical Engineers, 91, 556–569. doi: 10.1016/j.jtice.2018.06.007.

[28] C.R. Legler, N.R. Brown, R.A. Dunbar, M.D. Harness, K. Nguyen, O. Oyewole, W.B. Collier (2015) Scaled quantum mechanical scale factors for vibrational calculations using alternate polarized and augmented basis sets with the B3LYP density functional calculation model, Spectrochimica Acta Part A: Molecular and Biomolecular Spectroscopy, 145, 15–24. doi: 10.1016/j.saa.2015.02.103

[29] X.L. Zhang, Z.H. Jiang, Z.P. Yao, Y. Song, Z.D. Wu (2009) Effects of scan rate on the potentiodynamic polarization curve obtained to determine the Tafel slopes and corrosion current density, Corrosion Science, 51(3), 581–587. doi: 10.1016/j.corsci.2008.12.005.

[30] K.F. Khaled (2010) Studies of iron corrosion inhibition using chemical, electrochemical and computer simulation techniques, Electrochimica Acta, 55(22), 6523–6532. doi: 10.1016/j.electacta.2010.06.027.

[31] E. Heraldy, Y. Hidayat, M. Firdaus (2016) The Langmuir isotherm adsorption equation: the monolayer approach, in: IOP Conference Series: Materials Science and Engineering, 107(1), 012067. doi: 10.1088/1757-899X/107/1/012067.

[32] H.S. Aljibori, A. Alamiery, T.S. Gaaz, W.K. Al-Azzawi (2024) Exploring corrosion protection for mild steel in HCl solution: An experimental and theoretical analysis of an antipyrine derivative as an anticorrosion agent, Carbon Neutralization, 3(1), 74–93. doi: 10.1002/cnl2.108.

[33] E. Ituen, O. Akaranta, A. James (2017) Evaluation of performance of corrosion inhibitors using adsorption isotherm models: an overview, Chemical Science International Journal, 18(1), 1–34. doi: 10.9734/CSJI/2017/28976.

[34] F.E. Abeng, V.D. Idim, O.E. Obono, T.O. Magu (2017) Adsorption and adsorption isotherm: application to corrosion inhibition studies of mild steel in 2 M HCl, World Scientific News, 77(2), 298–313.

[35] C.G. Vaszilcsin, M.V. Putz, A. Kellenberger, M.L. Dan (2023) On the evaluation of metal-corrosion inhibitor interactions by adsorption isotherms, Journal of Molecular Structure, 1286, 135643. doi: 10.1016/j.molstruc.2023.135643.

[36] K.G. Prajapati, P.S. Desai (2025) Corrosion inhibition of aluminum alloy in HCl by SDS: experimental, SEM/AFM imaging, and computational insights (DFT and MD simulations), Journal of Molecular Modeling, 31(6), 172. doi: 10.1007/s00894-025-06391-y.

[37] U. Habeeba, N. Raghavendra (2025) A theoretical approach to the corrosion inhibition of iron (110) in HCl activation by environmental benign four amino acids: MC simulation and DFT studies, Extreme Materials, 1(2), 1–10. doi: 10.1016/j.exm.2025.02.001

[38] R.G. Parr, R.G. Pearson (1983) Absolute hardness: companion parameter to absolute electronegativity, Journal of the American Chemical Society, 105(26), 7512–7516. doi: 10.1021/ja00364a005.

[39] I.B. Obot, D.D. Macdonald, Z.M. Gasem (2015) Density functional theory as a tool for corrosion inhibitor design, Corrosion Science, 99, 1–30. doi: 10.1016/j.corsci.2015.01.037.

[40] K.A. Othman, W.M. Hamad, R.A. Omer (2025) Theoretical and experimental exploration of organic molecules adsorption on iron surfaces for corrosion inhibition: a review, Corrosion Reviews, 43(3), 335–359. doi: 10.1515/corrrev-2024-0039.

[41] Jamil DM, Al-Okbi AK, Hanon MM, Rida KS, Al-Amiery AA, Alkaim AF, Kadhim A, Kadhum AA. Carbethoxythiazole corrosion inhibitor: as an experimentally model and DFT theory. Journal of Engineering and Applied Sciences. 2018;13(11):3952-9. doi: 10.3923/jeasci.2018.3952.3959.

[42] M. El Faydy, A. Barrahi, N. Timoudan, I. Warad, Z. Safi, N. Wazzan, G. Kaichouh, F. Benhiba, A. Dafali, B. Lakhrissi, A. Zarrouk (2026) Corrosion inhibition and adsorption behaviour of two novel quinolin-8-ols on carbon steel surface in HCl: synthesis, electrochemical, surface characterisation, and quantum chemical approaches, Canadian Metallurgical Quarterly, 3;65(2):1629-51. doi: 10.1080/00084433.2025.2508104

[43] A. Recherache, F. Benghanem, L. Toukal, N. Bounedjar, M. Foudia, B. Abebe, M.W. Alam (2025) Electrochemical, quantum chemical, and thermodynamic investigation of a Schiff base corrosion inhibitor for XC70 steel, Scientific Reports, 15(1), 19350. doi: 10.1038/s41598-025-04051-y.

[44] Z.A. Betti, H.H. Al-Doori, A.F. Mahmood, A.A. Alamiery (2025) Corrosion inhibition of mild steel in 1 M HCl using 5-(3-Methylphenyl)-4-((4-Nitrobenzylidene) amino)-4H-1,2,4-Triazole-3-Thiol: Experimental and theoretical insights, Progress in Color, Colorants and Coatings, 18(4), 461–477. doi. 10.30509/pccc.2025.167462.1359

[45] A.M. Resen, M.M. Hanoon, W.K. Alani, A. Kadhim, A.A. Mohammed, T.S. Gaaz, A.A. Kadhum, A.A. Al-Amiery, M.S. Takriff (2021) Exploration of 8-piperazine-1-ylmethylumbelliferone for application as a corrosion inhibitor for mild steel in hydrochloric acid solution, International Journal of Corrosion and Scale Inhibition, 10(1), 368–387. doi: 10.17675/2305-6894-2021-10-1-21.

[46] F. Bentiss, M. Traisnel, M. Lagrenee (2000) The substituted 1,3,4-oxadiazoles: a new class of corrosion inhibitors of mild steel in acidic media, Corrosion Science, 42(1), 127–146. doi: 10.1016/S0010-938X(99)00049-9

[47] R. Ballinas-Indili, P. Roncagliolo-Barrera, R. Salcedo, F.J. Rodríguez-Gómez, C. Álvarez-Toledano (2025) Ultrasound-assisted synthesis of 2-Benzylidene-1-Indanone derivatives and evaluation as a corrosion inhibitor for mild steel in 1 M HCl solution, ACS Omega, 10(21), 21147–21161. doi: 10.1021/acsomega.4c09705.

[48] G. Bereket, C. Öğretir, Ç. Özşahin (2003) Quantum chemical studies on the inhibition efficiencies of some piperazine derivatives for the corrosion of steel in acidic medium, Journal of Molecular Structure: THEOCHEM, 663(1–3), 39–46. doi: 10.1016/j.theochem.2003.08.062.

[49] N. Jaàfar, H. El Alaoui El Abdallaoui, H. El Attari, A. Matine, M.M. Rguiti, H.A. Sir, S. Jebbari, M. Hilali (2023) Experimental and theoretical studies on corrosion inhibition of mild steel in molar hydrochloric acid solution by a newly benzimidazole derivative, Journal of Bio- and Tribo-Corrosion, 9(3), 59. Doi. 10.1007/s40735-023-00775-4

[50] A. Popova, M. Christov, T. Deligeorgiev (2003) Influence of the molecular structure on the inhibitor properties of benzimidazole derivatives on mild steel corrosion in 1 M hydrochloric acid, Corrosion, 59(9), 756–764. Doi. 10.5006/1.3277604

[51] K.F. Khaled (2006) Experimental and theoretical study for corrosion inhibition of mild steel in hydrochloric acid solution by some new hydrazine carbodithioic acid derivatives, Applied Surface Science, 252(12), 4120–4128. doi: 10.1016/j.apsusc.2005.06.016.

[52] B.I. Ita, E. Offiong (2000) Inhibitation of mild steel corrosion in hydrochloric acid by 2-aminopyridine and 2-(aminomethyl) pyridine, Global Journal of Pure and Applied Sciences, 6(1), 51–56.

[53] E.E. Oguzie (2005) Corrosion inhibition of mild steel in hydrochloric acid solution by methylene blue dye, Materials Letters, 59(8–9), 1076–1079. doi. 10.1016/j.matlet.2004.12.009.

IZVOD

EKOLOŠKI KOMPATIBILNA ZAŠTITA MEKOG ČELIKA U 1 M HCL KORIŠĆENJEM N-(ORTO-ANIZIL)PIPERAZINA: SINERGISTIČKI ELEKTROHEMIJSKI I DFT PRISTUP

Korozivno ponašanje mekog čelika u 1 M HCl ispitivano je u prisustvu N-(orto-anizil)piperazina (NAP), heterocikličnog organskog inhibitora, korišćenjem elektrohemijskih metoda, analize površine i kvantno hemijskog modeliranja. Studije potenciodinamičke polarizacije (PDP) pokazale su da NAP deluje kao inhibitor mešovitog tipa, postižući efikasnost inhibicije do 84% pri koncentraciji od 0,5 mM. Adsorpcija NAP-a na površini čelika pratila je ponašanje Langmirove izoterme, što ukazuje na pokrivenost monoslojem i spontanu adsorpciju, potkrepljenu negativnom Gibsovom slobodnom energijom od –30,03 kJ•mol^{-1}. Skenirajuća elektronska mikroskopija (SEM) potvrdila je značajno smanjenje karakteristika površinske korozije u prisustvu NAP-a. Proračuni teorije funkcionala gustine (DFT) pokazali su povoljne elektronske deskriptore, uključujući visok HOMO (–7,927 eV), nizak LUMO (1,307 eV) i pozitivnu frakciju prenosa elektrona (DN = 0,398), što podržava jake interakcije donor-akceptor sa površinom mekog čelika. Parametri molekularne mehanike ukazali su na stabilnu strukturnu fleksibilnost idealnu za adsorpciju. Predložen je sveobuhvatni mehanizam inhibicije koji uključuje i fizisorpciju i hemisorpciju. Studija ističe NAP kao ekološki prihvatljiv i efikasan inhibitor korozije, nudeći sinergijsko razumevanje inhibicije kroz eksperimentalne i teorijske pristupe.

Ključne reči: *Piperazin, potenciodinamička polarizacija, inhibitor korozije, SEM, DFT*

Naučni rad
Rad primljen: 26.08.2026.
Rad korigovan: 28.04.2026.
Rad prihvaćen: 07.05.2026.

Wael. H. Alsaedi: https://orcid.org/0009-0009-2715-4468
Ahmed Al-Amiery: https://orcid.org/0000-0003-1033-4904